Available online at www.sciencedirect.com
SCIENCE DIRECT®
Physics of the Earth and Planetary Interiors 139 (2003) 21–34
PHYSICS OF THE EARTH AND PLANETARY INTERIORS
www.elsevier.com/locate/pepi

Effect of pressure on Fe–Mg interdiffusion in $(Fe_xMg_{1-x})O$, ferropericlase

C. Holzapfel*, D.C. Rubie, S. Mackwell[1], D.J. Frost

Bayerisches Geoinstitut, Universität Bayreuth, D-95440 Bayreuth, Germany

Received 24 November 2002; received in revised form 9 March 2003; accepted 10 March 2003

Abstract

Fe–Mg interdiffusion in ferropericlase has been studied at pressures between 8 and 23 GPa and temperatures between 1653 and 2073 K, using a multianvil apparatus. The compositions of the single crystal diffusion couples were $X_{FeO} = 0.07$ for one crystal and $X_{FeO} = 0.37$ for the other, although in one case pure MgO was used instead of $X_{FeO} = 0.07$. Fe–Mg interdiffusion at oxygen fugacities buffered by Ni–NiO, including 1 bar data at 1673 and 1873 K of Mackwell et al. (in preparation), can be described for $0.07 < X_{FeO} < 0.37$ by:

$$D_{Fe\text{–}Mg} = D_0 \exp\left(\frac{AX_{FeO}}{RT}\right) \exp\left(-\frac{E_A + V_A P}{RT}\right)$$

where the pre-exponential factor $D_0 = 9.8(\pm 0.7) \times 10^{-6}\,m^2\,s^{-1}$, the constant $A = 132 \pm 13\,kJ\,mol^{-1}$, the activation energy $E_A = 255 \pm 16\,kJ\,mol^{-1}$, the activation volume $V_A = 3.3 \pm 0.1\,cm^3\,mol^{-1}$, X_{FeO} is mole fraction of FeO in $(Fe_xMg_{1-x})O$, T is absolute temperature, and P is pressure. This result can be used to constrain Fe–Mg interdiffusion coefficients of ferropericlase in the Earth's lower mantle. At the top of the lower mantle, at 23 GPa and 2000 K, diffusivities will be $0.5 \times 10^{-13}\,m^2\,s^{-1}$ and $1.1 \times 10^{-13}\,m^2\,s^{-1}$ for $X_{FeO} = 0.1$ and 0.2, respectively. Extrapolating the results to higher pressures suggests that diffusive interaction at the core–mantle boundary will extend at most ~15 km into the lower mantle.

Keywords: Diffusion; Activation volume; Ferropericlase; Multianvil; Lower mantle; Core–mantle boundary

1. Introduction

Ferropericlase is believed to be the second most abundant phase in the Earth's lower mantle and forms by disproportionation of ringwoodite into silicate perovskite and ferropericlase at the 660 km discontinuity (Liu, 1975; Guyot et al., 1988; Madon et al., 1989). Hence, ferropericlase is one of the most abundant constituent minerals of our planet. An understanding of the diffusion properties of this phase is therefore necessary for constraining processes such as mantle convection, homogenization of chemical heterogeneities, interaction with metal during core formation, and the extent of reactions occurring at the core–mantle boundary.

Most studies of diffusion in the system MgO–FeO have been performed on the end member MgO. Reviews of Mg and O self-diffusion data at 1 bar and

* Corresponding author. Tel.: +49-921-55-3746; fax: +49-921-55-3769.
E-mail address: christian.holzapfel@uni-bayreuth.de (C. Holzapfel).
[1] Present address: Lunar and Planetary Institute, 3600 Bay Area Blvd, Houston, TX 77058-1113, USA.

0031-9201/$ – see front matter © 2003 Elsevier B.V. All rights reserved.
doi:10.1016/S0031-9201(03)00142-0

variable temperatures can be found in Freer (1980) and Wuensch (1983). Vočadlo et al. (1995) investigated ionic diffusion in MgO by computer calculations via lattice dynamics. Only a few studies exist on Fe–Mg interdiffusion in the system MgO–FeO. Experiments employing polycrystalline diffusion couples or single crystals embedded in powders were performed by Bygdén et al. (1997), Rigby and Cutler (1965) and Blank and Pask (1969). The temperature range of these experiments was restricted to 1363–1588 K. The oxygen fugacity was not buffered directly and led to discrepancies in the results (see Bygdén et al. (1997) for a discussion and comparison).

Mackwell et al. (in preparation) performed Fe–Mg interdiffusion experiments employing single crystal diffusion couples over a wide range of temperatures and oxygen fugacities at 1 bar. From their results, diffusion depends on oxygen fugacity with an exponent of 0.22 and exponentially on composition, although their equation also includes a compositional dependence in the pre-exponential factor. A pure exponential compositional dependence was observed for Fe–Mg interdiffusion by Bygdén et al. (1997), for Ni tracer diffusion from thin films into NiO–MgO single crystal solid solutions by Wei and Wuensch (1973) and in interdiffusion studies of NiO–MgO by Blank and Pask (1969), Appel and Pask (1971), and Jakobsson (1996).

To understand transport processes in the lower mantle, where ferropericlase is an important constituent phase, diffusivities as a function of pressure are needed. $(Fe_xMg_{1-x})O$ ferropericlase is well suited for high pressure experiments due to the large stability field of this phase. Ita and Cohen (1997, 1998) performed a theoretical study on diffusion in pure MgO at high pressures. Calculated self-diffusion coefficients for Mg and O decrease with increasing pressure. Van Orman et al. (2002) performed multianvil experiments to measure Mg, Al and O self-diffusion in MgO between 15 and 25 GPa at a constant temperature of 2273 K. Their results agree with the theoretical work of Ita and Cohen (1998) and the experimentally determined activation volume for Mg diffusion is 3.0 cm^3/mol.

In this study we present results of Fe–Mg interdiffusion experiments at temperatures of 1653–2073 K and pressures of 8–23 GPa along the Ni–NiO oxygen buffer. The starting compositions of the single crystals used as diffusion couples in this study were $X_{FeO} = 0.07$ or pure MgO and $X_{FeO} = 0.37$, where X_{FeO} denotes the mole fraction of FeO. The results are used to constrain chemical diffusivity in (Mg, Fe)O ferropericlase solid solutions under conditions of the lower mantle.

2. Experimental technique

2.1. Crystal preparation

Commercially available single crystals of pure MgO (10 mm × 10 mm × 0.5 mm, purchased from Alfa AESAR), with one side oriented along (1 0 0), were used as starting materials for preparing the single crystal (Mg, Fe)O diffusion couples. FeO was diffused into the MgO crystals by annealing them in a (Mg, Fe)O powder inside an alumina crucible for 200 h at 1723 K and at an oxygen fugacity of 1.6 log units below the Ni–NiO buffer (NNO-1.6), using a CO/CO_2 gas-mixing furnace (approximate ratio of gas volumes: $CO/CO_2 = 0.25$). The (Mg, Fe)O powder had been synthesized previously by mixing laboratory grade Fe_2O_3 and MgO in an agate mortar followed by annealing for two cycles at 1673 K and an oxygen fugacity of NNO-1.6 for 20 h, with regrinding between the cycles.

After the diffusive enrichment of the single crystal slices in FeO, the sintered oxide powder was carefully ground away, maintaining the crystal orientation within 0.5° of (1 0 0), as determined by X-ray diffraction. However, because the diffusion coefficient is a second rank tensor and ferropericlase is cubic in the investigated pressure and temperature regime, there is no anisotropy in (Mg, Fe)O with respect to diffusion, and crystal orientation should not affect the results of the experiments (Nye, 1985).

The diffusion interface was polished with alumina powders to 0.3 μm. For the high-pressure diffusion experiments, discs of 1 mm diameter and 500 μm thickness were drilled out as starting crystals. Electron microprobe traverses over the samples showed heterogeneities of less than ±1.5 mol% FeO along the entire length of the crystal and less than ±0.25 mol% over 1 mm (diameter of diffusion couples). Alumina contamination from the reaction crucibles was not detected. However, on one side of the low iron content crystal a well sintered layer with polycrystalline

(Mg, Fe)O with the same composition and a Ca_2SiO_4 phase was observed after the experiments, possibly due to contamination during sample preparation.

2.2. High pressure experiments

The high pressure experiments were performed in a 1000 t Kawai-type multianvil press. For diffusion experiments at 8 and 12 GPa a 14/8 type multianvil assembly was used and above 16 GPa a 10/4 multianvil assembly was used (Fig. 1). These assemblies consist of a Cr_2O_3-doped MgO octahedral pressure medium with either 14 or 10 mm edge length and WC cubes with 8 or 4 mm edge length corner truncations. Fig. 1 shows the arrangement of the diffusion couple in the assembly. A straight $LaCrO_3$ resistance heater was used for heating the 10/4 cell, whereas in the 14/8 cell a stepped $LaCrO_3$ heater was employed to reduce temperature gradients along the capsule. The temperature was measured by a $W_{97}Re_3$–$W_{75}Re_{25}$ thermocouple without any correction for the effect of pressure. To prevent thermocouple poisoning with Ni from the sample capsule, a thin MgO disc was inserted between the capsule and the thermocouple.

For preparation of the sample capsule, Ni foil was rolled into a cylinder and then one end was folded over. After careful cleaning in an ultrasonic bath the single crystals were inserted, NiO powder (dried at 1000 °C) and a small Ni disc were added and the capsule was closed. Subsequently the capsule was stored in a desiccator until it was inserted into the assembly.

All parts of the assembly that consist of MgO, $LaCrO_3$ or Al_2O_3 were dried for at least 30 min at 1000 °C. In the 10/4 assembly the length of the thermocouple rod was chosen such that the thermocouple junction and the diffusion interface were arranged symmetrically around the hot spot. In the 14/8 assembly the thermocouple junction was located at the center of the assembly where thermal gradients are low. The complete assemblies were stored in a vacuum oven at 220 °C to prevent any absorption of water prior to the high pressure experiments.

For the 14/8 assembly, sample pressure was calibrated against hydraulic oil pressure at 1473 K using the coesite $\rightleftharpoons$ stishovite (Zhang et al., 1996) and the Mg_2SiO_4 $\alpha \rightleftharpoons \beta$ (Morishima et al., 1994) phase transformations. For the 10/4 assembly, pressure calibration at 1873 K was based on phase boundaries of $\gamma \rightleftharpoons$ perovskite + MgO, $\beta \rightleftharpoons \gamma$ and $\alpha \rightleftharpoons \beta$ in Mg_2SiO_4 (Suzuki et al., 2000; Akaogi et al., 1989; Morishima et al., 1994) as well as the ilmentite $\rightleftharpoons$ perovskite phase boundary in the system $MgSiO_3$ (Ono et al., 2001). The pressure uncertainty is estimated to be ±0.5 GPa. After pressurization, the

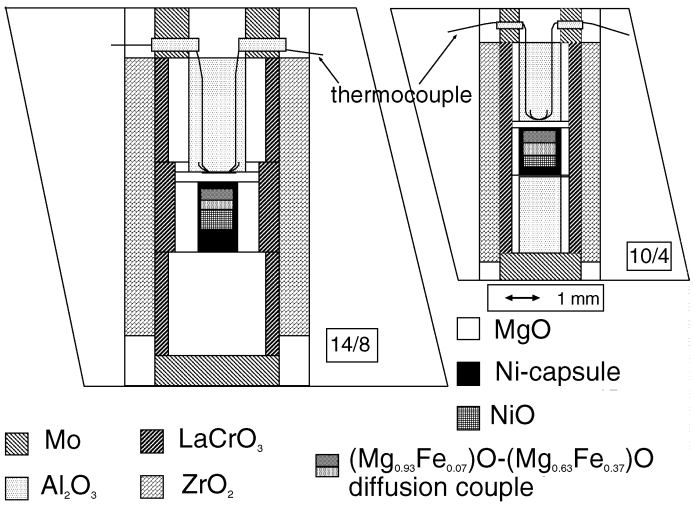

Fig. 1. Pressure assemblies for multianvil experiments used in this study. At $P < 16$ GPa a 14/8 assembly (14 mm edge length of the octahedron, WC cubes with 8 mm edge length corner truncations) and at $P \geq 16$ GPa a 10/4 assembly were used. The sample capsule consists of Ni foil with the addition of NiO to buffer fO_2.

sample was heated to the desired temperature which was maintained for a time period that resulted in a diffusion profile length of ∼100 μm. In order to quench the experiments the power to the furnace was switched off, resulting in a drop in temperature to <300 °C in less than 2 s. Each recovered octahedron was mounted in epoxy and was ground down until the middle of the capsule was exposed.

3. Analytical procedure

Fig. 2 shows a backscattered electron image of a diffusion couple annealed for 45 min at 16 GPa and 1873 K. The two halves of the diffusion couple are generally well sintered after the diffusion experiments. Fractures are rare and when present were carefully avoided during electron microprobe analysis.

Fe–Mg concentration profiles have been measured by electron microprobe using a Cameca SX-50 equipped with four wavelength dispersive spectrometers. The accelerating voltage was either 15 or 20 kV and the probe current was 20 nA. Measurement times on peak and background were 20 and 10 s, respectively, resulting in a detection limit of approximately 2500 ppm for Fe and 600 ppm for Mg. Under these conditions ferropericlase is stable and no Mg loss occurred. As standards, either enstatite or MgO were used for Mg and either metallic Fe or Fe_2O_3 were used for Fe, depending on which combination gave totals closest to 100 wt.% on both crystals.

To determine the Fe^{3+} content of the samples, Mössbauer analysis was performed on sample C55, annealed at 2073 K and 23 GPa for 21 min, using a thin section of 100 μm thickness. The Fe^{3+} content was approximately 2–3 at.% of the total Fe content. The same sample was also used for Fourier transform infrared spectroscopy. Only the low Fe-content crystal could be examined because of severe absorption on the Fe-rich side. Most analysis points gave a H_2O content of around 12 ppm; only one measurement point near the edge of the sample showed 60 ppm of H_2O. The total water content is therefore low and consistent with previous water solubility measurements (Bolfan-Casanova et al., 2002).

4. Diffusion coefficient determination

An example of a diffusion profile is shown in Fig. 3. Due to the strong dependence of diffusivity on composition and the large compositional difference between

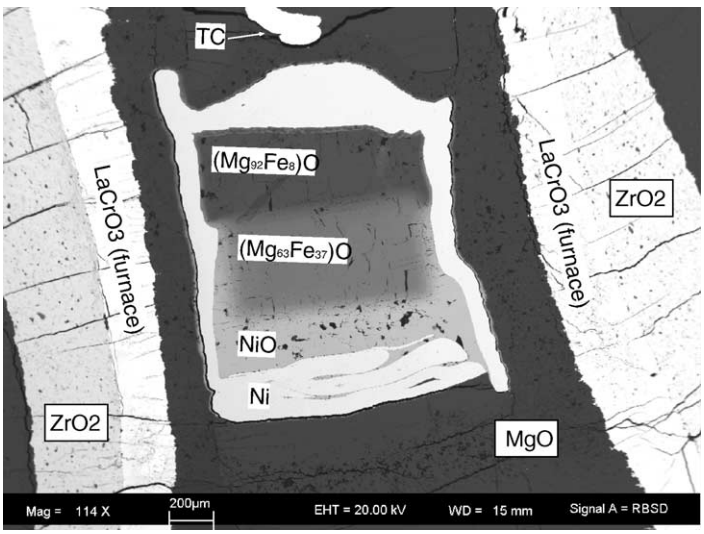

Fig. 2. Backscattered electron image of the pressure assembly after a ferropericlase diffusion experiment. Conditions of the experiment were 16 GPa and 1873 K with an annealing time of 45 min. The diffusion couple is seen surrounded by the Ni capsule. The NiO used for buffering fO_2 also interacted chemically with the end of the diffusion couple over a distance of ∼150 μm.

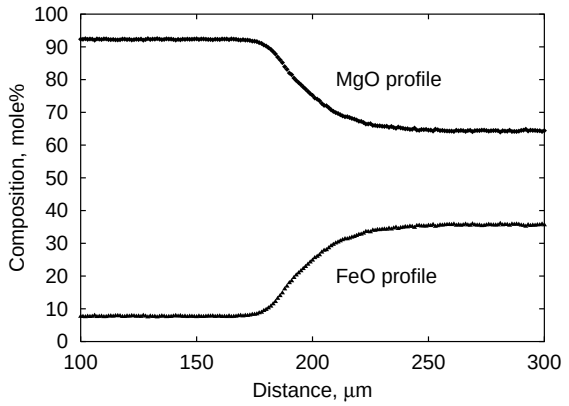

Fig. 3. Diffusion profile that developed at 23 GPa and 1656 K after 961 min. The asymmetry due to the compositional dependence of diffusivity is clearly visible. The flat parts of the profile, towards each end, are indicative of the original homogeneity of the crystals.

the two crystals ($0.08 < X_{FeO} < 0.37$), the profile is asymmetric. There is no direct analytical solution to the diffusion equation where the diffusivity depends on composition. To analyze the composition dependence two alternative methods were applied.

The Boltzmann–Matano analysis is an exact formulation that describes the diffusion coefficient in terms of the derivative and the integral of the concentration–distance function (Shewmon, 1989):

$$D(c^*) = -\frac{1}{2t}\left(\frac{\mathrm{d}x}{\mathrm{d}c}\right)_{c^*} \int_{c=0}^{c^*} x\,\mathrm{d}c \tag{1}$$

where $D(c^*)$ is the diffusion coefficient at concentration c^*, t the duration of the diffusion anneal, x the position along the profile, and c the concentration. For computing the derivative in Eq. (1) from the experimental data, a smoothing function is required. Different functions, normally used for sigmoidal growth models (Ratkowsky, 1983), were applied. Due to the strong nonlinearity of these functions, precise fitting can be problematic. The resulting best-fit obtained by the nonlinear least squares fit routine of Mathematica (Version 4.1.0.0, Wolfram Research) is shown in Fig. 4, together with diffusion coefficients calculated as a function of composition.

The alternative approach is to use a numerical finite difference scheme with an assumed composition dependence. At 1 bar, Fe–Mg interdiffusion in ferropericlase can be described by:

$$D_{\mathrm{Fe\text{–}Mg}} = (D_{01} + D_{02} f\mathrm{O_2}^m X_{\mathrm{FeO}}{}^p) \times \exp\left(-\frac{E_A - \alpha X_{\mathrm{FeO}}}{RT}\right) \tag{2a}$$

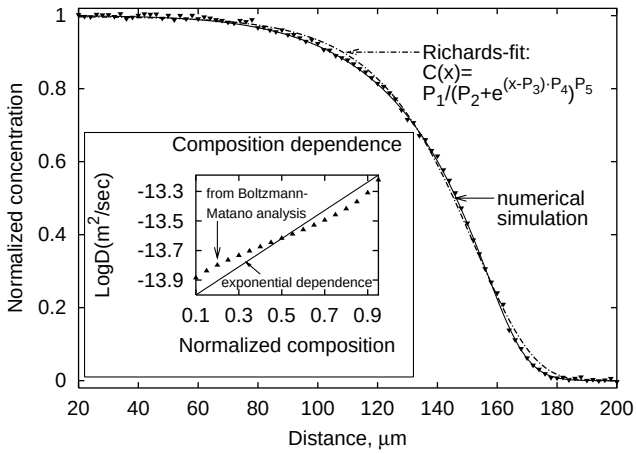

Fig. 4. Determination of Fe–Mg interdiffusion coefficients from an asymmetric normalized FeO diffusion profile in ferropericlase. Normalization was performed such that the concentration X_{FeO} is equal to one at the left end of the profile and zero at the right end of the profile. The profile was measured after an experiment at 23 GPa and 1851 K for 183 min. The lines show the numerical simulation (solid line) and the fitted empirical sigmoidal function (dashed line), employing a Richards-type function (Ratkowsky, 1983), which was used for the Boltzmann–Matano analysis. The results are given in the inset and are consistent within the experimental error of ±0.3 log units.

where $D_{01} = 1.8 \times 10^{-8}\,m^2\,s^{-1}$, $D_{02} = 1.1 \times 10^{-4}\,m^2\,s^{-1}$, the activation energy $E_A = 206\,500\,J\,mol^{-1}$, $\alpha = 61\,950\,J\,mol^{-1}$, $m = 0.22$, $p = 1.17$, R is the molar gas constant, and T is temperature. This equation was derived by Mackwell et al. (in preparation) using point defect arguments and the values of the parameters are best-fit values to their data. The power law dependence only plays a significant role at low iron concentration, whereas for compositions with $X_{FeO} > 0.07$, diffusivities are primarily exponentially dependent on composition, and Eq. (2a) can be approximated at constant temperature by:

$$D = D_0 \exp(ac(x)) \tag{2b}$$

where $c(x)$ is the concentration at distance x, the constant a controls the extent of asymmetry observed in the diffusion profiles and the pre-exponential factor includes the temperature and oxygen fugacity of the experiment which are constants for each individual experiment. Also for olivine (Morioka and Nagasawa, 1991) a pure exponential dependence on composition was observed. For all experiments employing diffusion couples with $X_{FeO} > 0.07$, Eq. (2b) is inserted into Fick's second law, giving:

$$\frac{\partial c}{\partial t} = \frac{\partial}{\partial x}\left(D_0 \exp(ac(x))\frac{\partial c}{\partial x}\right) \tag{3}$$

which after differentiation gives:

$$\frac{\partial c}{\partial t} = aD_0 \exp(ac(x))\left(\frac{\partial c}{\partial x}\right)^2 + D_0 \exp(ac(x))\frac{\partial^2 c}{\partial x^2} \tag{4}$$

The partial derivatives in this equation were approximated by finite differences and the solution propagated in time using an explicit formulation (Smith, 1985). Simulations to the profiles were performed by varying the parameters in Eq. (2b) to minimize the sum of squared residuals between calculated and observed composition values along the profile. In Fig. 4 the resulting fit to the experimental data is shown in comparison with the nonlinear fit used for Boltzmann–Matano analysis.

The inset of Fig. 4 shows a comparison of the diffusion coefficients determined using both types of analysis. Because of the assumed exponential compositional dependence for the numerical approximation, the logarithm of the diffusion coefficient follows a straight line when plotted against composition. The diffusion coefficients calculated by the Boltzmann–Matano analysis deviate systematically towards higher diffusivities at low Fe-concentrations and lower diffusivities at high Fe-concentrations, compared to the numerical model. Most of this deviation can be attributed to the smoothing function itself, which does not fit the profile perfectly at low and high iron concentrations. However, the difference is at most 0.1 log units for diffusion couples with $0.07 < X_{FeO} < 0.37$ and therefore lies well within the overall experimental error. Hence both methods can be used to give consistent results for these experiments. For sample C64, in which an MgO single crystal was used as one end member, the numerical model, using only an exponential compositional dependence (Eq. (2b)), slightly overestimates diffusivities at the MgO-rich end of the profile. In this region the composition power law dependence contributes significantly to the diffusivity (Mackwell et al., in preparation). This implies a change in the charge neutrality condition for point defects when approaching the MgO-rich end of the solid solution. Based on the above comparisons, all diffusion coefficients presented below were derived using the numerical model.

5. Results

The initial compositions of the crystals and the experimental conditions are listed in Table 1. The composition-dependent diffusivity was simulated for each diffusion profile by the numerical method outlined above and fitted parameters for the constants D_0 and a in Eq. (2b) are also listed in Table 1. As pointed out above, sample C64, employing pure MgO as one end member, could not be simulated satisfactorily at the MgO-rich end using a pure exponential composition dependence because the power law term in Eq. (2a) becomes significant. Therefore, the profiles for this sample were reanalyzed with a composition dependence of $D = (D_0 + D_1(X_{FeO})^{1.17}) \exp(aX_{FeO})$ (cf. Eq. (2a)), where the constant a was fixed at a constant value of 4, consistent with the results at 1 bar (Mackwell et al., in preparation), and the constants D_0 and D_1 were allowed to vary. The result of this simulation is also given in Table 1.

To test the inter-experiment reproducibility a time series of experiments was performed at constant

Table 1
Experimental conditions, initial compositions of diffusion couples, parameters D_0, D_1 and a for the equation $D = (D_0 + D_1(X_{FeO})^{1.17}) \exp(aX_{FeO})$ (cf. Eq. (2a)), and Fe–Mg interdiffusion coefficients for $X_{FeO} = 0.2$[a]

Sample	P (GPa)	T (K)	Time (min)	X_{FeO} (crystal 1)	X_{FeO} (crystal 2)	D_0 ($\mu m^2/s$)	D_1 ($\mu m^2/s$)	a	log(D), $X_{FeO} = 0.2$
C48	23	2063	40	0.079	0.363	0.037	0	7.23	−12.80
C51	23	1851	183	0.080	0.370	0.0048	0	7.49	−13.67
C53	23	1656	961	0.077	0.359	0.000454	0	6.82	−14.75
C55	23	2073	21	0.079	0.362	0.035	0	7.38	−12.81
C62	16	1873	45	0.082	0.356	0.053	0	7.54	−12.62
C64	8	1873	20	0.00	0.354	0.0168	1.20	4.00	−12.35
C67	8	1873	5	0.087	0.350	0.12	0	8.92	−12.15
C68	12	1673	48	0.085	0.354	0.0063	0	10.66	−13.27
C72	12	1873	20	0.077	0.335	0.042	0	8.87	−12.60
C73	23	1923	46	0.082	0.340	0.028	0	7.41	−12.91
C81	8	1873	15	0.086	0.363	0.132	0	8.66	−12.13

[a] D_1 was only fitted for sample C64 in which pure MgO was one end member. For all other results the power law contribution of the compositional dependence is not significant; D_1 was therefore set to 0 (Eq. (2b)). All values are averages of simulations of at least two profiles measured on each sample. As an example Fe–Mg interdiffusion coefficients for $X_{FeO} = 0.2$ are given in the last column.

temperature of 1873 K and constant pressure of 8 GPa (Fig. 5). The three experiments were performed for 5, 15 and 20 min using different heating rates, multianvil presses and types of diffusion couples. No systematic variation of diffusivity as a function of time was observed and the overall scatter of the data was found to be better than ±0.3 log units. Therefore, at these conditions no zero-time effect due to heating was observed experimentally.

The composition-dependent Fe–Mg interdiffusion coefficient D at high pressure can be described by:

$$D = D_0 \exp\left(\frac{AX_{FeO}}{RT}\right) \exp\left(-\frac{E_A + (P - P_{ref})V_A}{RT}\right) \quad (5)$$

where the constant A describes the compositional dependence, X_{FeO} the mole fraction of FeO, V_A the

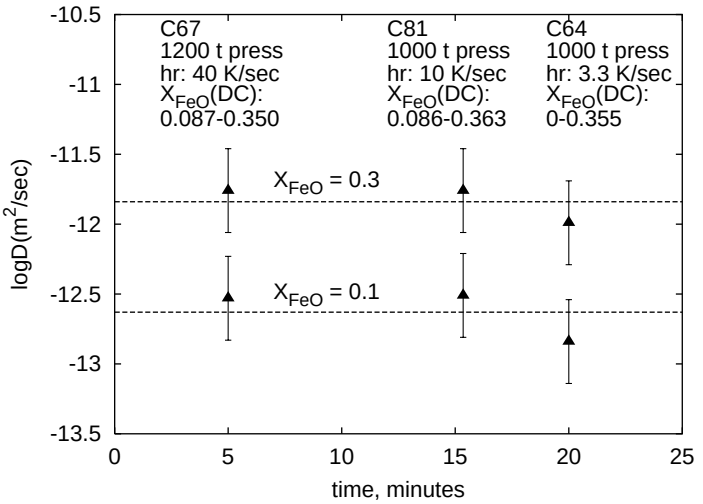

Fig. 5. Logarithm of the diffusion coefficient at constant temperature of 1873 K and constant pressure of 8 GPa. The dashed lines show the average values of diffusivity, recalculated for $X_{FeO} = 0.1$ and 0.3. The time series shows that the effects of the variation of heating rate (hr), multianvil press (1000 or 1200 t), and compositions of the diffusion couples (DC) on the results are negligible.

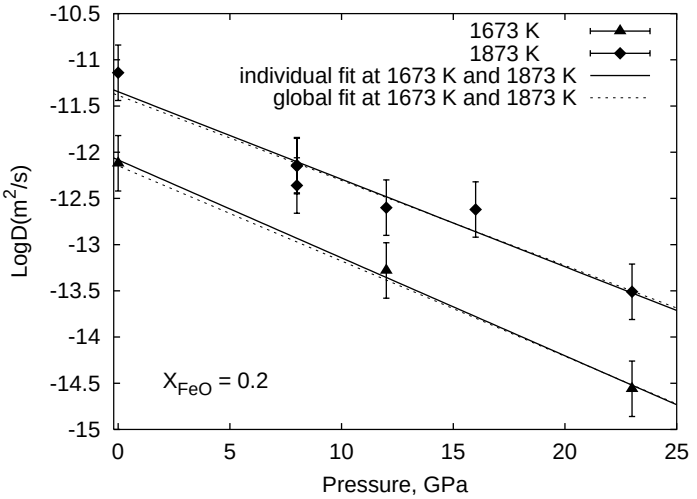

Fig. 6. Pressure dependence of diffusivity at 1673 and 1873 K and a constant composition of $X_{FeO} = 0.2$ (using data from Table 1). Data at 1 bar are from Mackwell et al. (in preparation). At 23 GPa, data-points are recalculated to 1673 and 1873 K from the correlation shown in Fig. 8. Individual fits to the data-points at each temperature, calculated using values from Table 1, are shown by the solid lines. The dotted lines show a global fit of Eq. (5) with the parameter values detailed in the text.

activation volume, E_A the activation energy, P the pressure, P_{ref} the reference pressure (=1 bar), and T the absolute temperature. As discussed by Poirier (2000) the pressure dependence of the entropic term is neglected in this formulation. Eq. (5) is consistent with Eq. (2a), derived from point defect considerations, as long as $X_{FeO} > 0.07$.

Figs. 6 and 7 show the pressure dependence of diffusion from which the value of the activation volume V_A (Eq. (5)) has been determined using the slope of

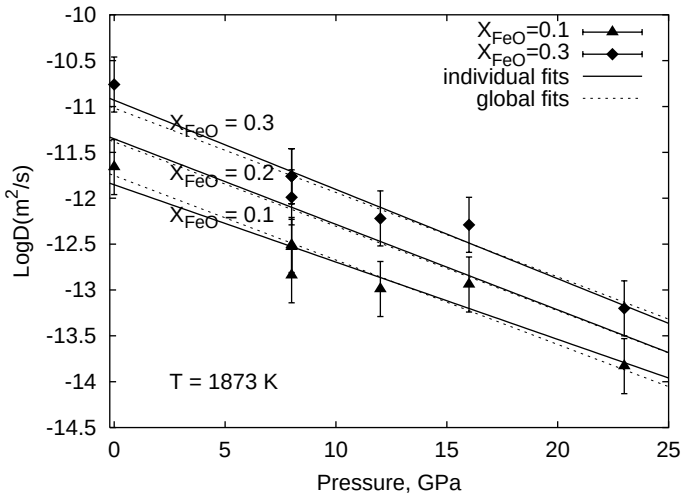

Fig. 7. Logarithm of the Fe–Mg interdiffusion coefficient as a function of pressure at a constant temperature of 1873 K recalculated for the compositions $X_{FeO} = 0.1$, 0.2, and 0.3 (Table 1). Data at 1 bar are from the study of Mackwell et al. (in preparation). At 23 GPa data-points are recalculated to 1873 K from the correlation shown in Fig. 8. Individual data-points are shown for $X_{FeO} = 0.1$ and 0.3. The solid lines are fits to the individual data-points at $X_{FeO} = 0.1$, 0.2, and 0.3 calculated from the values in Table 1. The dotted lines show the global fit of Eq. (5).

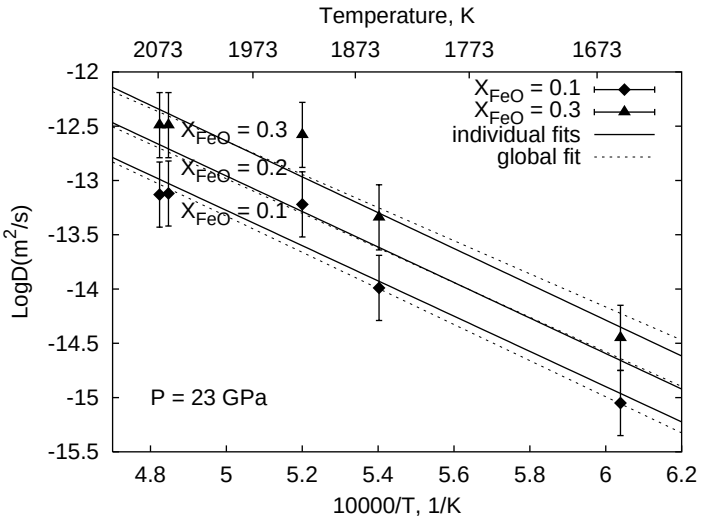

Fig. 8. Logarithm of the diffusion coefficient as a function of inverse temperature. Individual data-points, recalculated for $X_{FeO} = 0.1$ and 0.3 using parameters listed in Table 1, are shown for experiments performed at 23 GPa and 1656–2073 K. In addition, for $X_{FeO} = 0.1$, 0.2, and 0.3, individual fits of the data-points at these conditions are shown by the solid lines. At the same conditions the results of the global fit (Eq. (5)) are shown by the dotted lines.

a linear regression. Diffusivities at different compositions were calculated for each experiment by using the constants a and D_0 in Eq. (2b) listed in Table 1. The constant a in Eq. (2b) corresponds to $A/(RT)$ in Eq. (5). At 23 GPa, Fe–Mg interdiffusion coefficients were recalculated to 1673 and 1873 K using the temperature dependence given in Fig. 8. At 8 GPa three experiments have been performed, one of them using a diffusion couple of a pure MgO single crystal as one end member (C64, Table 1) and two employing a diffusion couple with $X_{FeO} = 0.09$ and $X_{FeO} = 0.35$ (C67). No significant differences in the diffusion coefficients derived using the different kinds of diffusion couples are observed (Fig. 5). Hence the result from C64 was included in all calculations presented below. From Fig. 6 values for the activation volume of 3.4 ± 0.5 and $3.3 \pm 0.5\,cm^3\,mol^{-1}$ at 1673 and 1873 K, respectively, are evaluated from the slopes of the regression lines. Fig. 7 shows that at 1873 K the activation volume is $3.0 \pm 0.5\,cm^3\,mol^{-1}$ at 10 mol% FeO, $3.3 \pm 0.5\,cm^3\,mol^{-1}$ at 20 mol% FeO and $3.5 \pm 0.5\,cm^3\,mol^{-1}$ at 30 mol% FeO. The error on the activation volume was estimated from the 1 sigma standard deviation of the fit of $\log D$ versus pressure at a fixed temperature and composition. Because the total variation is not larger than the 1 sigma standard deviation, it is concluded that at the experimental conditions the activation volume does not depend significantly on either temperature or composition.

The activation energy E_A at 23 GPa can be calculated using the calculated activation volume and the average constant A determined using Table 1 where A (Eq. (5)) $= a$ (Table 1, Eq. (2b)) $\times RT$, which at 23 GPa is $1.16 \times 10^5\,J\,mol^{-1}$, from a plot of $\log D$ against $10^4/T$ (Fig. 8). At 23 GPa, the activation energy is $253 \pm 50\,kJ\,mol^{-1}$ for $X_{FeO} = 0.1$, $260 \pm 53\,kJ\,mol^{-1}$ for $X_{FeO} = 0.2$, and $271 \pm 55\,kJ\,mol^{-1}$ for X_{FeO}=0.3.

As stated in the analytical section the crystal with $X_{FeO} = 0.07$ had some $CaO–SiO_2$ contamination on one surface. This surface was always on the opposite side of the crystal to the diffusion interface. Results obtained from sample C64, which did not employ this crystal, and from samples C72 and C73, where the contamination layer was removed prior to the diffusion anneal are consistent with the other experiments. Therefore, the contamination has no effect on the determined diffusion coefficients.

Using data recalculated to $X_{FeO} = 0.1$, 0.2 and 0.3 (Table 1) and including 1 bar data at 1673 and 1873 K from Mackwell et al. (in preparation), a global fit of Eq. (5) was performed, leading to $A = 132 \pm 13\,kJ\,mol^{-1}$, activation energy $E_A = 255 \pm 16\,kJ\,mol^{-1}$,

activation volume $V_A = 3.3 \pm 0.1\,cm^3\,mol^{-1}$, and the pre-exponential factor $D_0 = (9.8 \pm 0.7) \times 10^{-6}\,m^2\,s^{-1}$. The quoted errors are standard errors from the Mathematica (Version 4.1.0.0, Wolfram Research) package LinearRegression. From the deviation of the calculated and experimentally determined values the overall error is estimated to be 0.3 log units. These values for Eq. (5) are valid for an oxygen fugacity corresponding to the Ni–NiO buffer as will be discussed below. The experimental conditions for deriving these parameters were pressures of 0–23 GPa and temperatures of 1656–2073 K.

The value of $3.3\,cm^3\,mol^{-1}$ is in good agreement with the activation volume of $3.0\,cm^3\,mol^{-1}$ determined for Mg tracer diffusion in the experiments of Van Orman et al. (2002).

6. Discussion

6.1. Temperature gradients

Temperature gradients in the 10/4 assembly can be as large as $100\,K\,mm^{-1}$ (Trønnes and Frost, 2002). For a profile length of around 100–150 μm the temperature variation along the diffusion profile is therefore on the order of 10–15 K. Numerical simulations by finite differences using Eq. (5), but allowing the temperature to vary linearly along the profile, show that effects of profile lengthening or shortening are negligible ($\ll$1 μm at the extreme ends of the profiles).

Aside from pure distortion due to a change of diffusivity, temperature gradients can potentially also lead to Soret diffusion. This effect would be different in the two assembly types used in this study because temperature gradients in the 14/8 cell are much smaller in comparison to the 10/4 cell. Therefore, a kink or discontinuity would appear in the pressure correlation if the Soret effect leads to a significant contribution of the diffusional flux. Such a kink is not observed however (Figs. 6 and 7), so significant Soret diffusion can be excluded.

6.2. Heating effects

Some diffusion inevitably occurs while the sample is being heated. However, at 1873 K and 8 GPa, results of the time series shown in Fig. 5 show that this has little or no effect on the derived diffusion coefficients at these conditions. The contribution to the diffusion profiles during heating at all conditions was simulated by finite differences using Eq. (5). In an initial heating phase the temperature was varied from room temperature to the final temperature using the actual heating rates of the experiments. The best-fit parameters for Eq. (5) were used for the activation volume and the activation energy. The constant A was recalculated from Table 1. These simulations show that diffusion profiles with lengths of several microns, depending on the heating rate, develop during initial heating. The difference between simulations employing these extended profiles as the initial condition and simulations using an ideal step function as the initial condition vanishes very quickly, however, with progressive diffusion. After less than 5 min no significant differences can be observed for the combinations of heating rate and high temperature annealing times used in this study. Therefore, the profiles observed in this work only contain information about the diffusional properties at high temperature and it is mathematically justified to use an ideal step function as the initial condition in the simulation of the profiles.

6.3. Oxygen fugacity

All experiments reported here have been performed in Ni capsules in contact with NiO powder (Fig. 2). Therefore, Eq. (5) is only valid at oxygen fugacities corresponding to the Ni–NiO buffer. Because fO_2 at the Ni–NiO buffer varies with temperature and pressure, this dependence is implicitly built into Eq. (5) (see also Chakraborty and Ganguly, 1991).

According to Mackwell et al. (in preparation), Fe–Mg interdiffusion in ferropericlase varies with fO_2 by the factor of $(fO_2)^{0.22}$. To test if the high-pressure, high-temperature dependence of Fe–Mg interdiffusion is independently consistent with the 1 bar data from Mackwell et al. (in preparation), Eq. (5) was refitted without including the 1 bar data. The difference between diffusivities calculated at 1 bar using the back extrapolation of the high pressure data, and those calculated from the results of Mackwell et al. (in preparation) at an fO_2 corresponding to the Ni–NiO buffer, ranges from 0.01 log units at 1673 K and $X_{FeO} = 0.1$ to 0.58 log units at 2073 K for $X_{FeO} = 0.3$. Considering the experimental error of 0.3 log

units and the fact that the experimental data are extrapolated over a pressure range of 8 GPa, these differences indicate good consistency between the high pressure results and data obtained at 1 bar.

6.4. Diffusion in (Mg, Fe)O in the lower mantle

Using the values obtained in this study it is possible to constrain rates of chemical diffusion in ferropericlase in the lower mantle. Based on studies of Fe–Mg partitioning between ferropericlase and silicate perovskite, X_{FeO} of ferropericlase in the lower mantle is likely to lie in the range 0.1–0.2 depending on the alumina content of coexisting silicate perovskite (Fei, 1999; Poirier, 2000; Frost and Langenhorst, 2002).

Using best-fit values for Eq. (5), the Fe–Mg interdiffusion coefficient is $1.1\times10^{-13}\,m^2\,s^{-1}$ for $X_{FeO} = 0.2$ and $0.5\times10^{-13}\,m^2\,s^{-1}$ for $X_{FeO} = 0.1$ at 23 GPa and 2000 K, corresponding to the top of the lower mantle. The pressure at the core–mantle boundary is approximately 136 GPa (Dziewonski and Anderson, 1981) but the temperature is poorly constrained. A value of 3000 K on the mantle side of the thermal boundary layer is derived from a mantle adiabat whereas for a core adiabat the temperature at the core–mantle boundary is likely to be around 5000 K (Poirier, 2000). Most of the parameters used in these estimations are highly uncertain but according to Williams (1998) a temperature contrast of 1000–2000 K across D'' is expected. For the estimation of diffusion coefficients at the core–mantle boundary 3000 and 5000 K are adapted as limiting cases. According to Boehler (1996) the melting temperature of ferropericlase at 136 GPa is also ∼5000 K.

Another uncertainty arises from the value of the activation volume in the lower mantle because theoretical considerations predict that it should decrease with increasing pressure (Karato, 1981; Poirier and Liebermann, 1984; Mills et al., 1991). Ita and Cohen (1997) calculated free energies of vacancy pair formation and migration of Mg and O in pure MgO at pressures from 0 to 140 GPa and temperatures from 1000 to 5000 K. Using these data together with calculated lattice parameters enabled these authors to calculate the decrease in the activation volume of the intrinsic Mg self-diffusion coefficient with increasing pressure. However, experimental and theoretical evidence shows that Mg diffusion in MgO occurs by an extrinsic diffusion mechanism at all experimental conditions so far investigated (Sempolinski and Kingery, 1980; Wuensch, 1983; Vočadlo et al., 1995; Van Orman et al., 2002). This is also likely to be the case for the Fe–Mg interdiffusion experiments reported in this study. Hence, to compare the results of Ita and Cohen (1997) with experimental results only the migration volume $V_m = \partial G_m/\partial P$, where G_m is the free energy of migration of the diffusion mechanism, has to be considered. The activation volume of $3.0\,cm^3\,mol^{-1}$ for Mg tracer diffusion determined by Van Orman et al. (2002) agrees well with the migration volume of $3.1\,cm^3\,mol^{-1}$ calculated employing free energies of migration by Ita and Cohen (1997) between 0 and 20 GPa at 2000 K. It will be assumed here that the data for the free energy of migration reported in Ita and Cohen (1997) can also be used to constrain the pressure dependence of the activation volume of $(Fe_xMg_{1-x})O$ ferropericlase at pressures greater than 23 GPa.

The migration entropy S_m calculated as $S_m = \partial G_m/\partial T$ from the values of Ita and Cohen (1997) is approximately constant between 0 and 140 GPa indicating that the pre-exponential factor is pressure independent. In this case the activation volume $V_a(P)$ at any pressure P and constant temperature is given by (Poirier, 2000):

$$V_a(P) = -RT\frac{\partial \ln D(P)}{\partial P} = \frac{\partial H_a(P)}{\partial P} \tag{6}$$

where $D(P)$ is the diffusion coefficient at pressure P and $H_a(P)$ the activation enthalpy at pressure P. As an approximation, the activation volume between 1 bar and pressure P was estimated from

$$V_a^{avg}(P) = \frac{H_a(P) - H_a\,(1\,bar)}{P - 1\,bar} \tag{7}$$

Values for the activation enthalpy $H_a(T, P)$ at temperature T and pressure P can be calculated employing the results of Ita and Cohen (1997) from $H_a(T, P) = G_m(T, P) + TS_m(P)$, where $G_m(T, P)$ is the migration free energy at temperature T and pressure P and $S_m(P)$ is the migration free entropy at pressure P. Between 0 and 140 GPa at 3000 K an average migration volume of $1.35\,cm^3\,mol^{-1}$ was derived in this way for extrinsic Mg self-diffusion. Assuming a similar pressure effect on the activation volume for Fe–Mg interdiffusion

Table 2
Diffusion coefficients at 136 GPa (core–mantle boundary pressure) derived using limiting assumptions for conditions prevailing at the core–mantle boundary as discussed in the text[a]

T_{CB} (K)	V_a ($cm^3\,mol^{-1}$)	X_{FeO}	D_{Fe-Mg} ($m^2\,s^{-1}$)	x_{diff} (km)
3000	1.4	0.1	3×10^{-13}	0.4
3000	1.4	0.2	5×10^{-13}	0.5
5000	1.4	0.1	3×10^{-10}	13
5000	1.4	0.2	4×10^{-10}	15

[a] V_a is the activation volume estimated using Eq. (7) and the calculations of Ita and Cohen (1997). Diffusion coefficients are calculated using best-fit values for Eq. (5) but employing the estimated activation volume of $1.4\,cm^3\,mol^{-1}$ instead of the low pressure value of $3.3\,cm^3\,mol^{-1}$. The length x_{diff} of diffusional interaction is calculated as $x_{diff} = 2\sqrt{Dt_e}$ where t_e is the age of the Earth (4.5×10^9 years).

leads to an average activation volume of $1.4\,cm^3\,mol^{-1}$ for calculation of diffusivities at the core–mantle boundary. Diffusion coefficients derived using a combination of the limiting assumptions listed above are given in Table 2.

The diffusion coefficients listed in Table 2 can be used to constrain the length of diffusion x_{diff} at the core–mantle boundary over the entire history of the Earth ($t_e = 4.5 \times 10^9$ years) by applying the equation $x_{diff} = 2\sqrt{Dt_e}$. The diffusional distance ranges between 0.5 and 15 km at 3000 and 5000 K, respectively. Due to the effect of oxygen fugacity on diffusion (Eq. (2a)) these length scales are upper limits because the fO_2 at the core–mantle boundary will be more reducing than the corresponding fO_2 of the Ni–NiO buffer, where the experiments of this study have been performed. These length scales are slightly longer than the estimates of Van Orman et al. (2002) using self-diffusion coefficients of Mg in MgO. If the data of Ita and Cohen (1997) are not applicable for Fe–Mg interdiffusion and the activation volume does not decrease with pressure then equilibration distances would be significantly shorter. Preliminary results for diffusion in Mg-silicate perovskite show that diffusion rates for Fe–Mg interdiffusion in this phase are orders of magnitude slower than for ferropericlase (Holzapfel et al., 2001). Thus, it can be concluded that pure diffusive interaction during Earth's history between the core and the mantle would not have any significant effect on the bulk compositions of these geochemical reservoirs.

7. Conclusions

In this study Fe–Mg interdiffusion in $(Fe_xMg_{1-x})O$ ferropericlase was investigated at high pressure using the multianvil technique. The resulting asymmetric composition profiles can be described well by numerical simulations using an exponential composition dependence of diffusion for $X_{FeO} > 0.07$. Including data obtained at 1 bar from Mackwell et al. (in preparation), diffusivities decrease monotonically at constant temperature, with a constant activation volume of $3.3\,cm^3\,mol^{-1}$ along the Ni–NiO buffer. The difference between diffusivities at 1 bar and 23 GPa is approximately 2.5 orders of magnitude at constant temperature. Therefore, in modeling processes occurring in the mantle that depend on diffusion, it is essential to take the effect of pressure into account.

It is expected that the absolute value of the activation volume decreases in the lower mantle. Taking this effect into account by using results from theoretical calculations (Ita and Cohen, 1997) leads to diffusion coefficients at the base of the lower mantle at 136 GPa and 3000 K which are approximately of the same order as at the top of the lower mantle (Table 2) despite the temperature increase of 1000 K. In the thermal boundary layer at the core–mantle boundary where temperatures most likely increase by 1000–2000 K, diffusivity is increased by approximately three orders of magnitude. Based on these estimates, diffusive interaction between the metallic core and the base of the lower mantle would develop over distances of 0.5–15 km over the entire history of the Earth. Taking into account the presence of silicate perovskite is likely to significantly reduce these distances.

Acknowledgements

We thank Hubert Schulze and Oskar Leitner for sample preparation, Heinz Fischer and Georg Hermannsdörfer for preparing the parts of the sample assemblies, Catherine McCammon for assisting with the Mössbauer milliprobe and Geoffrey Bromiley for help with the FTIR analysis. We also thank J. Van Orman for helpful discussions and J. Brady, E.B. Watson and J. Van Orman for constructive reviews that greatly improved the manuscript.

References

Akaogi, M., Ito, E., Navrotsky, A., 1989. Olivine-modified spinel–spinel transitions in the system Mg_2SiO_4: calorimetric measurements, thermochemical calculation and geophysical application. J. Geophys. Res. 94, 15671–15685.

Appel, M., Pask, J.A., 1971. Interdiffusion and moving boundaries in NiO–CaO and NiO–MgO single-crystal couples. J. Am. Ceram. Soc. 54, 152–158.

Blank, S.L., Pask, J.A., 1969. Diffusion of iron and nickel in magnesium oxide single crystals. J. Am. Ceram. Soc. 52, 669–675.

Boehler, R., 1996. Melting of mantle and core materials at very high pressures. Phil. Trans. Roy. Soc. A 354 (1711), 1265–1278.

Bolfan-Casanova, N., Mackwell, S., Keppler, H., McCammon, C., Rubie, D.C., 2002. Pressure dependence of H solubility in magnesiowüstite up to 25 GPa: implications for the storage of water in the Earth's lower mantle. Geophys. Res. Lett. 29. 10.1029/2001GL014457.

Bygdén, J., Jakobsson, A., Sichen, D., Seetharaman, S., 1997. Interdiffusion studies in the system MgO–FeO. Z. Metallkd. 88, 433–437.

Chakraborty, S., Ganguly, J., 1991. Compositional zoning and cation diffusion in garnets. In: Ganguly, J. (Ed.), Diffusion, Atomic Ordering and Mass Transport: Selected Topics in Geochemistry. Springer, Berlin. Adv. Phys. Geochem. 8, 120–175.

Dziewonski, A.M., Anderson, D.L., 1981. Preliminary reference Earth model. Phys. Earth Planet. Inter. 25, 297–356.

Fei, Y., 1999. Solid solutions and element partitioning at high pressures and temperatures. In: Hemley, R.J. (Ed.), Physics and Chemistry of the Earth's Deep Interior. Mineral. Soc. Am., Rev. Mineral. 37, 343–367.

Freer, R., 1980. Bibliography: self-diffusion and impurity diffusion in oxides. J. Mater. Sci. 15, 803–824.

Frost, D.J., Langenhorst, F., 2002. The effect of Al_2O_3 on Fe–Mg partitioning between magnesiowüstite and magnesium silicate perovskite. Earth Planet. Sci. Lett. 199, 227–241.

Guyot, F., Madon, M., Peyronneau, J., Poirier, J.P., 1988. X-ray microanalysis of high-pressure/high-temperature phases synthesized from natural olivine in a diamond anvil cell. Earth Planet. Sci. Lett. 90, 52–64.

Holzapfel, C., Rubie, D.C., Frost, D.J., Langenhorst, F., 2001. EOS Trans. AGU 82 (Abstract: V51A-0967).

Ita, J., Cohen, R.E., 1997. Effects of pressure on diffusion and vacancy formation in MgO from nonempirical free-energy integrations. Phys. Rev. Lett. 79, 3198–3201.

Ita, J., Cohen, R.E., 1998. Diffusion in MgO at high pressure: implications for lower mantle rheology. Geophy. Res. Lett. 25, 1095–1098.

Jakobsson, A., 1996. Diffusion studies in the system NiO–MgO using high temperature X-ray technique. Z. Metallkd. 87, 55–60.

Karato, S., 1981. Rheology of the lower mantle. Phys. Earth Planet. Int. 24, 1–14.

Liu, L.G., 1975. Post-oxide phases of forsterite and enstatite. Geophys. Res. Lett. 2, 417–419.

Mackwell, S., Bystricky, M., Sproni, C., in preparation. Fe–Mg interdiffusion in (Mg, Fe)O. Phys. Chem. Mineral.

Madon, M., Guyot, F., Peyronneau, J., Poirier, J.P., 1989. Electron microscopy of high-pressure phases synthesized from natural olivine in diamond anvil cell. Phys. Chem. Mineral. 16, 320–330.

Mills, D.R., Parker, S.C., Wall, A., 1991. The effect of pressure on Schottky pair formation in MgO—a lattice dynamic approach. Phil. Mag. A 65 (5), 1133–1144.

Morioka, M., Nagasawa, H., 1991. Ionic diffusion in olivine. In: Ganguly, J. (Ed.), Diffusion, Atomic Ordering and Mass Transport. Springer, Berlin. Adv. Phys. Geochem. 8, 176–197.

Morishima, H., Kato, T., Suto, M., Ohtani, E., Urakawa, S., Utsumi, W., Shimomura, O., Kikegawa, T., 1994. The phase boundary between α- and β-Mg_2SiO_4 determined by in situ X-ray observation. Science 265, 1202–1203.

Nye, J.F., 1985. Physical Properties of Crystals. Oxford Science Publications, Oxford, 329 pp.

Ono, S., Katsura, T., Ito, E., Kanzaki, M., Yoneda, A., Walter, S., Urakawa, W., Utsumi, K., Funakoshi, K., 2001. In situ observation of ilmentite–perovskite phase transition using synchrotron radiation. Geophys. Res. Lett. 28, 835–838.

Poirier, J.-P., 2000. Introduction to the Physics of the Earth's Interior. Cambridge University Press, Cambridge, 312 pp.

Poirier, J.-P., Liebermann, R.C., 1984. On the activation volume for creep and its variation with depth in the Earth's lower mantle. Phys. Earth Planet. Int. 35 (4), 283–293.

Ratkowsky, D.A., 1983. Nonlinear Regression Modeling. Dekker, New York, 276 pp.

Rigby, E.B., Cutler, I.B., 1965. Interdiffusion studies of system Fe_XO–MgO. J. Am. Ceram. Soc. 48, 95–99.

Sempolinski, D.R., Kingery, W.D., 1980. Ionic conductivity and magnesium vacancy mobility in magnesium oxide. J. Am. Ceram. Soc. 63, 664–669.

Shewmon, P., 1989. Diffusion in Solids. The Minerals, Metals & Materials Society, Warrendale, Pennsylvania, 246 pp.

Smith, G.D., 1985. Numerical Solution of Partial Differential Equations—Finite Difference Methods. Clarendon Press, Oxford, 337 pp.

Suzuki, A., Ohtani, E., Morishima, H., Kubo, T., Kanbe, Y., Kondo, T., Okada, T., Terasaki, H., Kato, T., Kikigawa, T., 2000. In situ determination of the phase boundary between wadsleyite and ringwoodite in Mg_2SiO_4. Geophys. Res. Lett. 27, 803–806.

Trønnes, R.G., Frost, D.J., 2002. Peridotite melting and mineral-melt partitioning of major and minor elements at 22–24.5 GPa. Earth Planet. Sci. Lett. 197, 117–131.

Van Orman, J.A., Fei, Y., Hauri, E.H., Wang, J., 2002. Diffusion in MgO at high pressures: constraints on deformation mechanisms and chemical transport at the core–mantle boundary. Geophys. Res. Lett. 30 (2), 1056. 10.1029/2002GL016343.

Vočadlo, L., Wall, A., Parker, S.C., Price, G.D., 1995. Absolute ionic diffusion in MgO—computer calculations via lattice dynamics. Phys. Earth Planet. Int. 88, 193–210.

Wei, G.C.T., Wuensch, B.J., 1973. Composition dependence of ^{63}Ni diffusion in single-crystal NiO–MgO solid solutions. J. Am. Ceram. Soc. 56, 562–565.

Williams, Q., 1998. The temperature contrast across D''. In: Gurnis, M., Wysession, M.E., Knittle, E., Buffett, B.A. (Eds.), The Core–Mantle Boundary Region. AGU Geodynamics Series, vol. 28, pp. 73–81.

Wuensch, B.J., 1983. Diffusion in stoichiometric close-packed oxides. In: Bénière, F., Catlow, C.R.A. (Eds.), Mass Transport in Solids. NATO ASI Series, vol. 97, pp. 353–370.

Zhang, J., Li, B., Utsumi, W., Liebermann, R.C., 1996. In situ X-ray observations of the coesite stishovite transition: reversed phase boundary and kinetics. Phys. Chem. Mineral. 23, 1–10.